# LANGMUIR

pubs.acs.org/Langmuir Article

# Carbon Nanodots Derived from Urea and Citric Acid in Living Cells: Cellular Uptake and Antioxidation Effect

Zuowei Ji, Ziyu Yin, Zhenquan Jia, and Jianjun Wei\*



Cite This: Langmuir 2020, 36, 8632-8640



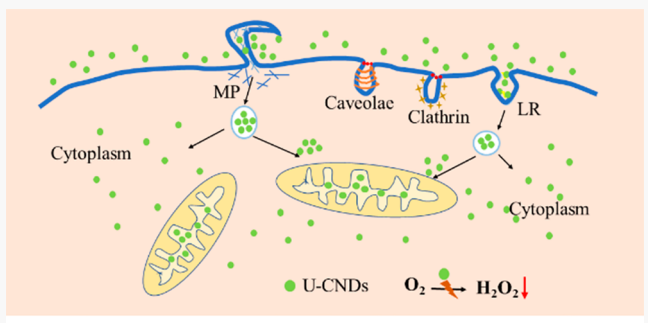
**ACCESS** 

Metrics & More

Article Recommendations

Supporting Information

ABSTRACT: Carbon nanodots (CNDs), reported as polyatomic carbon domains surrounded by amorphous carbon frames, have drawn extensive attention due to their easy-to-synthesis, outstanding electronic properties, and superior biocompatibility. However, substantial assessments regarding their biological performance are still needed, considering the complex nature of this type of relatively new nanoparticles. In this report, CNDs derived from urea and citric acid (U-CNDs) are investigated in the treatment of two cell lines, EA.hy926 and A549 cells, to examine the biocompatibility, cellular uptake, and antioxidation effect. The intracellular uptake study suggests an energy-dependent transport process into the cells mainly involving macropinocytosis and lipid raft-mediated endocytosis pathways. Moreover, the U-CNDs mostly target the mitochondria and present strong antioxidative



MP: Macropinocytosis Caveolae: Caveolae-mediated endocytosis LR: Lipid raft-mediated endocytosis Clathrin: clathrin-mediated endocytosis

effects by scavenging reactive oxygen species (ROS) in cells. Overall the findings in this report manifest that the U-CNDs could serve as a bioimaging reagent and antioxidant causing little deleteriousness in the respects of viability, plasma membrane integrity, and mitochondrial activity in both cell lines, and demonstrate some efficacy for inhibiting the metabolic activities of A549 cancer cells at higher concentration.

# **■ INTRODUCTION**

Particles range from 1 to 100 nm, having at least two dimensions are defined as nanoparticles (NPs). Intriguingly, NPs with a reduction in size exhibit distinctive physicochemical and biological properties compared to their conventional bulk materials. With the intensive study of NPs and rapid development of nanotechnology, the commercial demand of NPs in multiple fields, such as electronics, energy harvesting, biosensing, biosensing, biomedical and pharmaceutical applications, has increased dramatically.

Among all these different types of NPs, carbon nanodots (CNDs), a rising star among carbon-based nanoparticles, have attracted extensive attention in recent years due to their ecofriendly fabrication, excellent photoluminescence, outstanding optoelectronic properties, and function-structure tunability for biological applications. To give a few examples, Yang et al. claimed the hybrid based on carbon quantum dot (CQDs) could serve as an efficient electrocatalyst for hydrogen evolution. According to the upconversion luminescence property of CQDs, some researchers have demonstrated the design of CQDs-based photocatalysts could harness the full spectrum of sunlight. Meanwhile, CNDs are emerging as one of the promising candidates in various biological applications, such as cellular imaging, biosensing, drug/gene delivery, antioxidation, and theranostics, etc. For instance, CNDs that could simultaneously achieve bioimaging and

cancer therapy have been reported.<sup>23,24</sup> More specifically, some researchers have developed CNDs with specific organelle-targeting ability for better and precise treatment. For example, mitochondria-targetable CNDs could differentiate cancerous cells from normal cells based on the different uptake efficiency.<sup>25</sup> Furthermore, the CNDs with mitochondrial targeting ability could also be used for mitochondria-based therapies.<sup>26</sup> Other than that, the ability of CNDs as drug carrier and gene carrier have also been successfully demonstrated by researchers.<sup>27,28</sup>

These studies have resultantly attracted increasing interest in the biocompatibility or toxicological effects of the CNDs on human health and the ecological environment due to their structural complexity and high reactivity. Different structures or composites of CNDs can trigger distinctive responses in physicochemical and biological settings regarding oxidative properties. In our recent studies, the antioxidation capacity of the U-CNDs (nitrogen-doped) and nitrogen, sulfur codoped

Received: May 30, 2020 Published: July 1, 2020





CNDs (N,S-CNDs) was proved by scavenging DPPH radical in a physicochemical setting, <sup>29–31</sup> but the N,S-CNDs stimulate strong prooxidative effect in living cells. <sup>32</sup> Moreover, Zeng and co-workers have demonstrated that the fluorescent U-CNDs bonded with drug molecules, which is stimuli-responsive, can serve as a targeted drug delivery system for localized cancer therapy by examining their *in vivo* antitumoral acitivity. <sup>33</sup>

It is of significance to investigate how the composites in CNDs influence interactions at different chemical or biological systems. To differentiate from previous N,S-CNDs,<sup>32</sup> one type of CND derived from urea and citric acid is the focus of this work (named as U-CNDs). Generally, U-CNDs are reported as nitrogen-doped, excitation wavelength dependent fluorescent dots with a size of 1-6 nm.34 The photoluminescence features of the U-CNDs are reported to be a cooperative contribution from a few photoemissive centers, i.e., graphite core, surface states, and molecular fluorophores. 35-37 The blue or green emissions are associated with small molecular residues linked to the surface of the U-CNDs depending on the synthetic conditions. The origin of the blue fluorescence is attributed to the presence of bonded citrazinic acid or its derivatives and  $n-\pi^*$  transitions at the dots' edge when the CNDs are synthesized in a sealed reactor. 38,39 The green fluorescence of the CNDs may be contributed from the bonded 4-hydroxy-1*H*-pyrrolo[3,4-*c*]pyridine-1,3,6(2*H*,5*H*)trione (HPPT) or its derivatives at the surfaces of the dots synthesized in an open vessel reactor (solvent-free) reported by Kasprzyk et al. 40 On the basis of the fluorescence property, researchers have reported their roles as optical probes for cell imaging and for the selective detection of hypochlorite, peroxynitrite, ferricyanide, or ascorbic acid at  $\mu M$  level. 35,41-4

In this work, we present a comprehensive study of the U-CNDs in the aspects of biocompatibility, bioimaging, endocytosis, and ROS scavenging at the cellular level, which are inadequately studied. A normal cell line, EA.hy926 endothelial cells, and a cancer cell line, Human lung epithelial cell A549, are used in this study. Remarkably, an endocytic pathway study suggests an energy-dependent internalization process of the U-CNDs to the cells mainly involving the macropinocytosis and lipid raft-mediated endocytosis. In contrast to N,S-CNDs, the U-CNDs display good antioxidant effect by scavenging ROS in living cells and high biocompatibility. Collectively, this study highlights the potential of using the CNDs as a bioimaging agent and antioxidation agent or drug carriers, synchronously, in the living cells through an active cellular uptake process.

# **■ EXPERIMENTAL SECTION**

CNDs Synthesis and Characterization. CNDs were synthesized using citric acid and urea as precursors by a microwave assisted method.<sup>44</sup> First, 1.0 g of urea (Aldrich) and 1.0 g of citric acid (ACROS Organics) were dissolved completely in 1.0 mL of deionized water and then heated in a microwave synthesizer (CEM Corp 908005 Microwave Reactor Discovery System) at a power of 300 W for 18 min. Afterward, the aqueous reaction mixture was separated from the large and aggregated particles by a centrifuge (Solvall Legend XFR Floor Model Centrifuge) at 3500 rpm for 15 min. The dark-brown homogeneous solution was further purified using a dialysis membrane (Fisher Scientific) with a molecular weight cutoff of 1000 Da. Then the resulting solution was dried using a freeze-dryer (Labconco Free Zone 6 Freeze-Dryer) to get the solid sample. The absorption spectrum and fluorescence of the CNDs at 0.05 mg/mL were measured by a UV-vis photospectrometer (Cary 6000i, Agilent) and a fluorometer (Cary Eclipse, Agilent), respectively.

**Cell Cultivation.** EA.hy926 endothelial cells and Human lung epithelial cell line AS49 purchased from ATCC were cultured with optimized DMEM (AddexBio) media and F-12K (Kaighn's Modification of Ham's F-12 medium) (ATCC, 30-2004) medium supplemented with 1% streptomycin-penicillin (Fisher Scientific) and 10% fetal bovine serum (Sigma-Aldrich), respectively. Cells were grown in tissue culture-treated flasks at 37 °C in a 5%  $\rm CO_2$  humidified incubator.

Cellular Uptake, Cell Morphology, Plasma Membrane Integrity, Mitochondria Morphology, and Cell Viability **Studies.** Cells were first plated on glass coverslips with a cell density of  $1 \times 10^5$  inside a 12-well tissue culture plate for 24 h. Then the cells were treated with the CNDs suspensions at 0.0, 0.4, and 0.8 mg/mL for 24 h, respectively. Afterward, the cells were washed with PBS (Thermo fisher, pH 7.4) twice and fixed with 4% paraformaldehyde solution (Sigma-Aldrich) for 15 min at room temperature. Subsequently, paraformaldehyde was rinsed off by phosphate buffer solution (PBS), and the coverslips were mounted on glass slides by mounting media (Polysciences, Inc.). After storing at 4 °C overnight in the dark, the samples were imaged with a Zeiss Z1 Spinning Disk Confocal Microscope under Brightfield channel for the morphology monitoring and DAPI channel for the detection of cellular uptake of CNDs, respectively. For the investigation of the plasma membrane damage, propidium iodide (PI, 7.5 µM, 10 min, Molecular Probes,  $\lambda_{ex}/\lambda_{em}$  at 535/617 nm, Sigma-Aldrich) and acridine orange (AO, 3 μM, 10 min, Molecular Probes, Sigma-Aldrich) were added after CNDs incubation. After rinsing the cells with PBS, the samples were observed with RHOD and FITC channels for the PI and AO detection, respectively. Meanwhile, cells treated with hydrogen peroxide (Sigma-Aldrich) were used as a negative control. Mitochondria were stained with MitoTracker Red CMXRos (1 µM, 10 min, 37 °C, Molecular Probes,  $\lambda_{ex}/\lambda_{em}$  at 579/599 nm, Fisher Scientific) after CNDs' treatment and were imaged with RHOD channel after washing steps to check their morphology change. The viability of our cell line was tested by trypan blue exclusion method. After cells were seeded and incubated for 24 h, cells were treated with various concentrations of CNDs for another 24 h. Then, cells were rinsed with PBS and then trypsinized. Then 0.4% trypan blue stock solution (Sigma-Aldrich) was mixed with the same volume of the cell suspension to get a 1:1 dilution. Next, a cell counter was used to calculate the viability of the cells.

Endocytosis Inhibition. The endocytosis pathway of CNDs was investigated by using various endocytosis inhibitors. First, cells were seeded in a 12-well tissue culture plate with a cell density of  $1 \times 10^5$  at 37 °C for 24 h. Afterward, cells were maintained at 4 °C or incubated with one of the chemicals (NaN<sub>3</sub> (10 mM), CPZ (10  $\mu$ M), M $\beta$ CD (5 mg mL<sup>-1</sup> for EA.hy926 and 7 mg mL<sup>-1</sup> for A549), genistein (185  $\mu$ M), or amiloride (200  $\mu$ M)) at 37 °C for 1 h. For the investigation of the increased endocytosis caused by CPZ and genistein, CPZ + amiloride + M $\beta$ CD or genistein + amiloride + M $\beta$ CD was added and incubated with the cells at 37 °C for 1 h. The concentration of these inhibitors was chosen according to literature, which has been proved the achievement of transport inhibition in different cell lines. 45-48 Then, 0.8 mg mL<sup>-1</sup> CNDs was added to each well, respectively. After 3 h of incubation, cells were rinsed three times with PBS and trypsinized. Lastly, the cellular fluorescence intensities were analyzed by fluorescence-activated cell sorting (FACS). All of the endocytosis inhibitors used in this experiment were purchased from Sigma-

3-(4,5-Dimethylthiazol-2yl)-2,5-Diphenyltetrazolium Bromide (MTT)-Based Assay. In brief, CNDs at concentrations ranging from 0.05 to 0.8 mg/mL in culture medium was added into cells precultured for 24 h in a 24-well plate and exposed for another 24 h. Afterward, the CNDs suspensions were substituted with 0.2 mg/mL MTT (99%, Fisher Scientific) solution and the cells were incubated for additional 2 h. After rinsing the cells with PBS, a DMSO solvent (Fisher Scientific) was added to dissolve the formazan crystal at room temperature for 5 min. Finally, the absorbance at wavelength of 570 nm of each well was measured by a BioTek microplate reader.

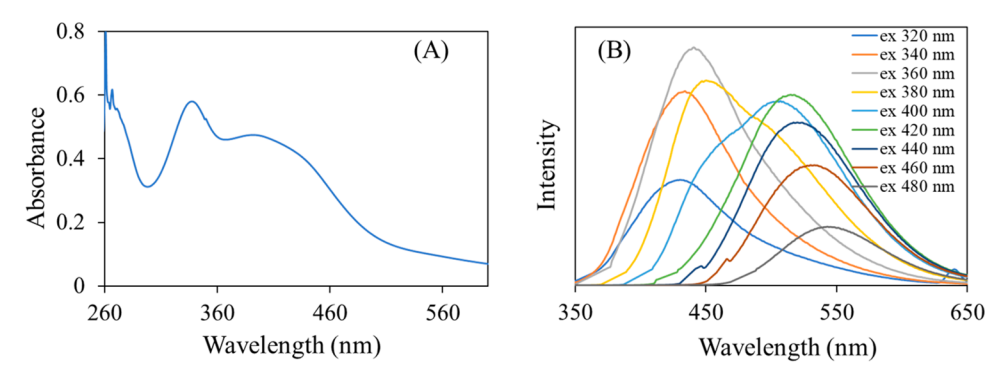


Figure 1. (A) Absorption spectrum and (B) Fluorescence emission spectra of the CNDs in deionized water.

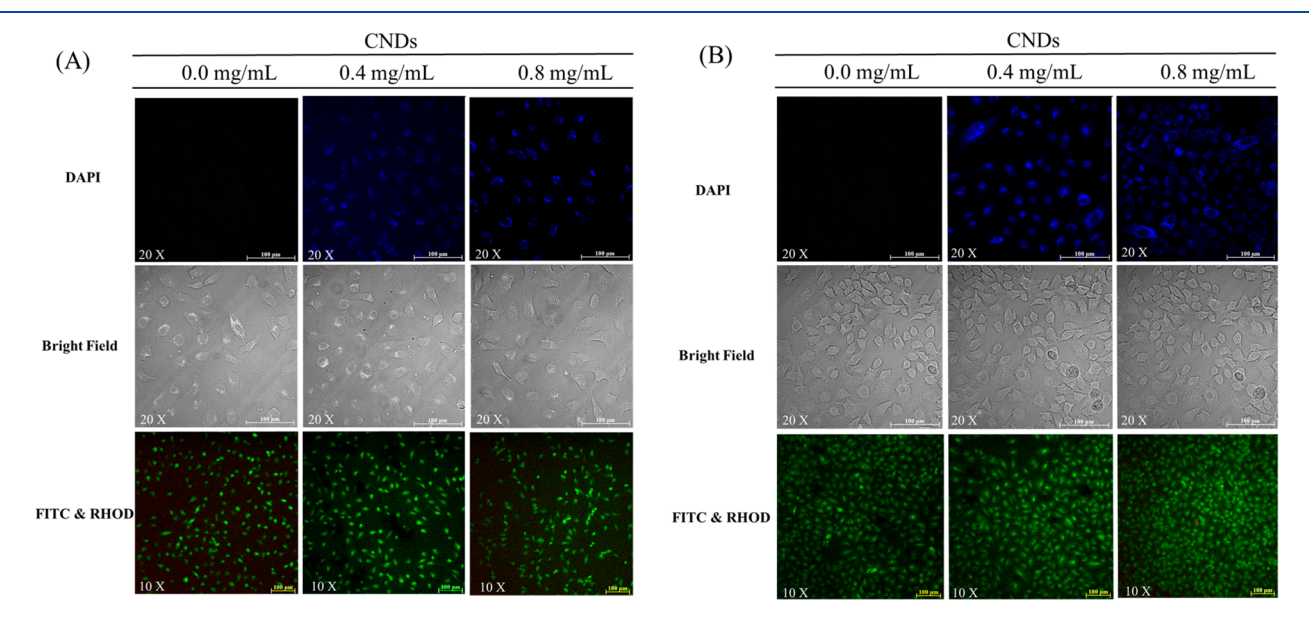


Figure 2. Confocal micrographs of cellular uptake, cell morphology, and plasma membrane integrity in EA.hy926 cells (A) and A549 cells (B) after incubation with CNDs for 24 h, respectively. All scale bar is  $100 \mu m$ .

Intracellular Reactive Oxygen Species (ROS) Analysis. Briefly, the cells with a density of  $1\times 10^4$  were first seeded in the 96-well plate and incubated for 24 h. Then the CNDs suspensions at different doses (0.1–0.8 mg/mL) were added to replace the medium. After 24 h exposure, the cells were rinsed three times with PBS. Thereafter, 5 and 15  $\mu$ M of 2′,7′-dichlorofluorescin diacetate (DCFH-DA, Sigma-Aldrich) diluted in FBS-free media was added to EA.hy926 endothelial cells and A549 cells, respectively. After 30 min incubation, the cells were rinsed twice with PBS. Finally, 100  $\mu$ L of PBS was added into each well, and fluorescence with  $\lambda_{ex}/\lambda_{em}$  at 485/528 nm of each well was measured by a BioTek microplate reader. In parallel, cells treated with L-ascorbic acid (AA, Sigma-Aldrich) at concentrations ranging from 0.1 to 0.8 mg/mL were used as positive controls.

Analysis of CNDs Subcellular Localization. First, cells were grown on glass coverslips with a cell density of  $1 \times 10^5$  inside a 12-well tissue culture plate for 24 h. CNDs suspensions with concentration of 0.0, 0.4, and 0.8 mg/mL were added to designated wells for 24 h, respectively. Then the mitochondria were labeled with MitoTracker Red CMXRos (0.1  $\mu$ M, 10 min, 37 °C, Molecular Probes,  $\lambda_{ex}/\lambda_{em}$  at 579/599 nm, Fisher Scientific). Before imaging, cells were washed twice with PBS. Subsequently, the cells on coverslips were imaged immediately with Zeiss Z1 Spinning Disk Confocal Microscope using a 63× oil immersion objective lens under DAPI channel for the CNDs and RHOD channel for the mitochondria at the same time. The concentrations of CNDs and MitoTracker Red were optimized, respectively, to eliminate interference.

**Statistical Analysis.** Data analysis was carried out using Microsoft Excel. Data was expressed as mean + standard deviation (SD) from three independent experiments. Asterisk was marked for differences at P < 0.05 compared to control groups in a one-tailed t test. The acquisition and analysis of confocal micrographs were done by Axiovision 4.8 software and ImageJ. Flowing Software 2.5.1 was used to analyze the data from FACS.

# ■ RESULTS AND DISCUSSION

Carbon nanodots (CNDs) using citric acid and urea as precursors were synthesized by a one-step microwave route.<sup>44</sup> Figure 1A depicts the absorption spectrum of the CNDs over the spectral range from 260 to 600 nm. The main peak at 340 nm represents the  $n-\pi^*$  transitions of the C= $\hat{O}$ . And Figure 1B exhibits the fluorescence emission of the CNDs within the excitation wavelength of 320 to 480 nm, and the quantum yield was obtained ~8.6% at 360 nm excitation. More detailed morphology and structure-property information was described in our recent publications. 25 The synthesis reproducibility of the U-CNDs is characterized by the UVvisible and fluorescence spectra as shown in Figure S1. The measured  $\zeta$  potential of the U-CNDs is  $-36 \pm 3$  mV at pH 7 in water, 51 indicating a good stability in aqueous solution. Reportedly, similar hydrothermal synthesis using citric acid and urea might produce small amount of free citrazinic acid.<sup>38</sup> Citrazinic acid has absorption peak around 340 nm and steady excitation independent fluorescence at peak 440 nm in water solution. We compared the excitation dependent fluorescence of U-CNDs after 1 day and 4-day dialysis. Insignificant influence was detected in regards to the fluorescence peak shift (data not shown), suggesting that free citrazinic acid in the U-CNDs was minimal.

Since the U-CNDs are emitting fluorescence, which makes it possible to detect the internalization of the CNDs into cells by confocal microscope under DAPI channel. In a follow-up study, the cell morphology and plasma membrane integrity were checked after incubation with 0.0, 0.4, 0.8 mg/mL U-CNDs for 24 h. Figure 2 shows the imaging results using two cell lines, EA.hy926 cells and A549 cells. From the bright field images in Figure 2, one can easily tell that no significant abnormality in both cell lines was observed after the U-CND treatments. Plasma membrane damage was assessed by using propidium iodide (PI), a red fluorescent nuclear stain that only enters dead cells with poor plasma membrane integrity. In other words, the PI in red color is an indicator of dead cells. In order to distinguish between the live and dead cells, Acridine Orange was selected to stain all nucleated cells to generate green fluorescence. While the U-CNDs may have somewhat overlap of the green fluorescence, it will not impact the red PI as an indicator for dead cells. As shown in FITC and RHOD images of Figure 2, the PI-positive cells (dead cells) after U-CND treatments for both cell lines are very rare and negligible compared to the control cells without adding U-CNDs. Meanwhile, cells treated with hydrogen peroxide (H<sub>2</sub>O<sub>2</sub>) were served as positive controls. Most cells are dead after 5 min H<sub>2</sub>O<sub>2</sub> treatment as indicated by the PI red staining, and the AO green fluorescence images indicate the presence of all cells (both the living and dead) after H<sub>2</sub>O<sub>2</sub> treatment (Figure S2).

In concert, cell viability was performed with the trypan blue exclusion method. The method is based on a principle that the living cells possess intact cell membranes that will exclude trypan blue stain, whereas dead cells will not. Therefore, the number of viable cells could be counted using a hemocytometer or cell counter, because a viable cell will have a clear cytoplasm and a nonviable cell will have a blue cytoplasm. Our experimental results indicate the U-CNDs have supreme biocompatibility. Figure 3 demonstrated that the viability of both cell lines maintains above 98% after 0.8 mg/mL of CNDs

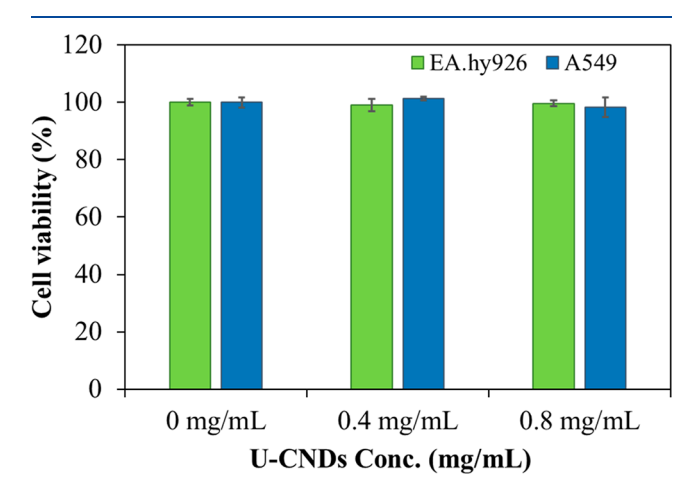
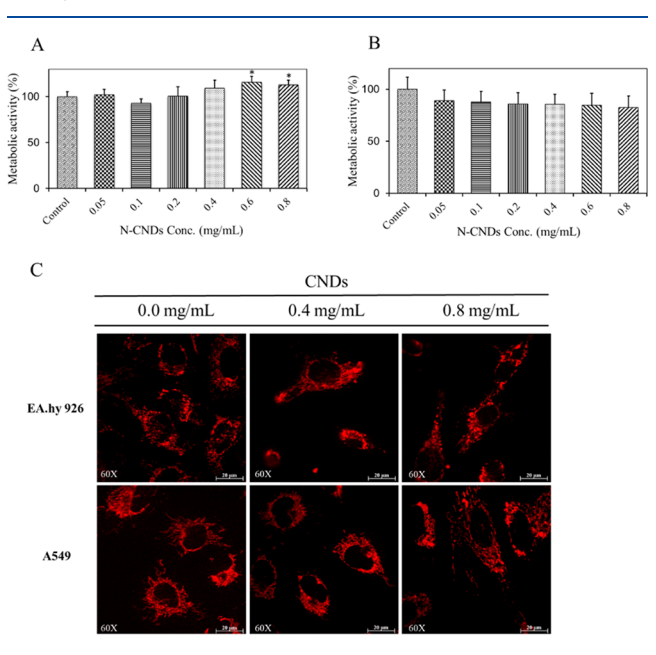


Figure 3. Cell viability of EA.hy926 and A549 cells detected by trypan blue exclusion method after incubation with CNDs for 24 h.

treatment for 24 h. Taken together, the U-CNDs cause negligible damage on cells at the concentrations that are sufficient for cell labeling.

Mitochondria are key organelles involved in numerous physiologically important processes. In addition to the generation of adenosine triphosphate (ATP), mitochondria are also involved in the regulation of cellular proliferation and cell cycle, apoptosis initiation, reactive oxygen species (ROS) generation, biomacromolecule synthesis, calcium signaling, and homeostasis. Mitochondrial dysfunction and damage are closely related to multiple common human diseases including Alzheimer's disease, amyotrophic lateral sclerosis, Parkinson's disease, heart disease, and Huntington's disease. Therefore, it is of considerable significance to evaluate the status of mitochondria such as their metabolic activities and morphology change.

Herein, colorimetric MTT (3-[4,5-dimethylthiazol-2-yl]-2,5-diphenyl tetrazolium bromide) assay and mitochondrial staining were performed to assess the status of the mitochondria in both cell lines after treatment of the U-CNDs. According to the mechanism of MTT assay, the insoluble purple formazan product reduced by the mitochondria of live cells can be dissolved by DMSO (dimethyl sulfoxide) and quantified using a microplate reader by measuring the absorbance at 570 nm. The results are presented in Figure 4. The decreased metabolic activity in A549 was



**Figure 4.** Mitochondria status evaluation after incubation with CNDs for 24 h. Metabolic activities of EA.hy926 cells (A) and A549 cells (B) treated with CNDs at different dosages for 24 h. (C) Mitochondria morphology of EA.hy926 cells and A549 cells after 24 h of incubation with CNDs at 0.4 and 0.8 mg/mL, respectively.

observed with increasing concentration of CNDs' treatment, ending up with a 17.5% decline at 0.8 mg/mL addition U-CND treatment, suggesting an inhibition of A549 cells by U-CND treatment. In contrast, the mitochondrial metabolic activity in EA.hy926 cells was found to be even more active than control cells after CNDs' treatment at higher concentrations. This study suggests that the U-CNDs may potentially have therapeutic effect on cancer cells. Meanwhile, effective fluorescence imaging of mitochondria, which enables monitor-

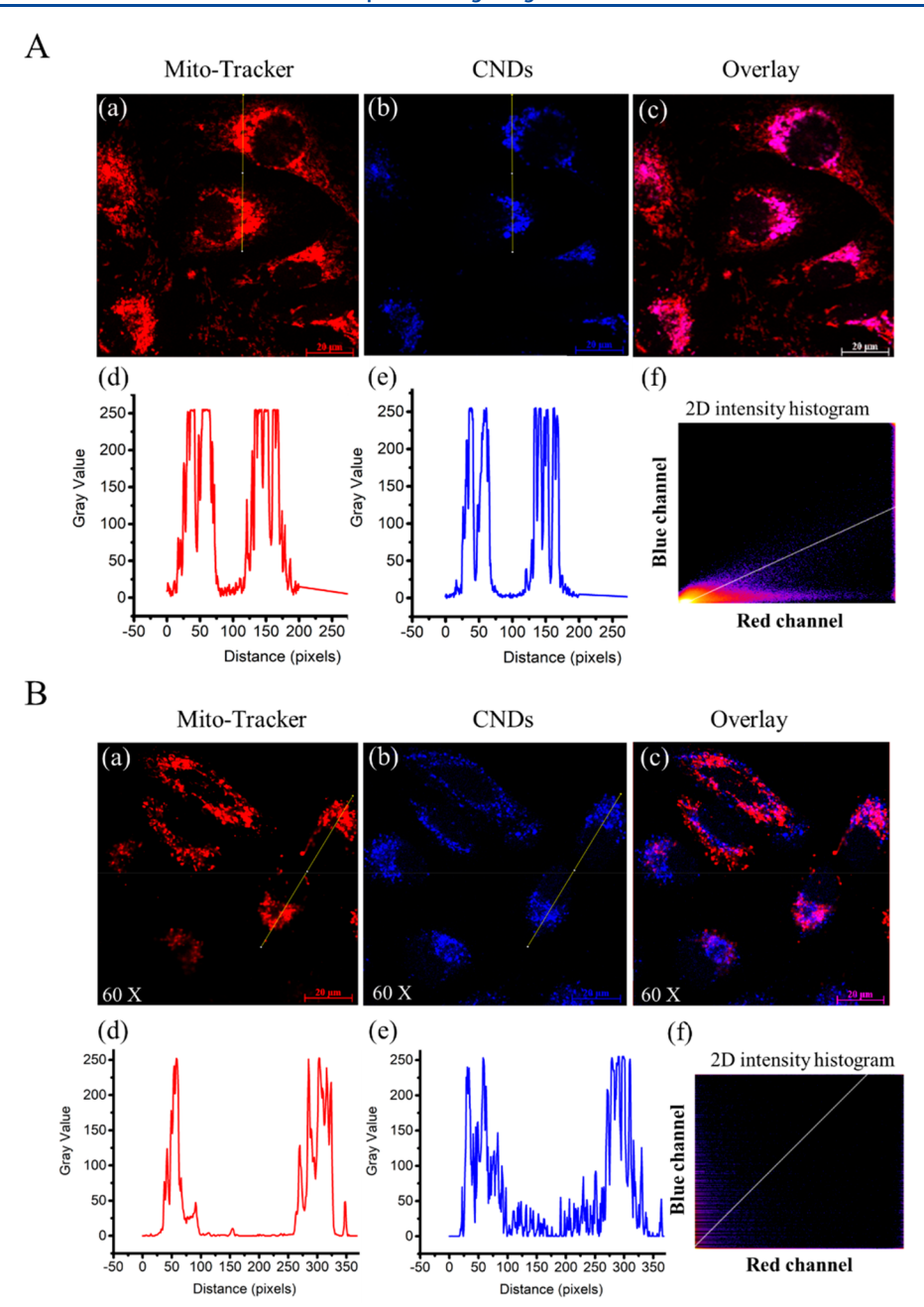


Figure 5. Subcellular localization of CNDs and their Fluorescence properties in EA.hy926 cells (A) and A549 cells (B). (a) Mito-Tracker Red staining. (b) Subcellular localization of CNDs. (c) Overlay of parts a and b. (d) and (e) The fluorescence intensity curves of the lines marked in parts a and b, respectively. (f) The intensity correlation plots of CNDs with Mito-Tracker Red in part c.

ing of the number, location, and state of mitochondria, was performed before and after the treatment by confocal microscope using MitoTracker Red, a dye specifically stains mitochondria in living cells. After comparison, no obvious mitochondrial damage, in the aspect of morphology, was observed after the U-CND's treatment in both cell lines.

Since the U-CNDs are of emissive fluorescence, one could explore their intracellular localization based on this property. Interestingly, it was found that the subcellular distribution of the U-CNDs mostly overlaps with stained mitochondria as shown in merged images (Figure 5a-c) as well as the overlapping plot profiles (Figure 5d,e) in both cell lines. Moreover, the 2D Histograms of image analysis (Figure 5f) provide a good way to visualize the correlation of the pixel

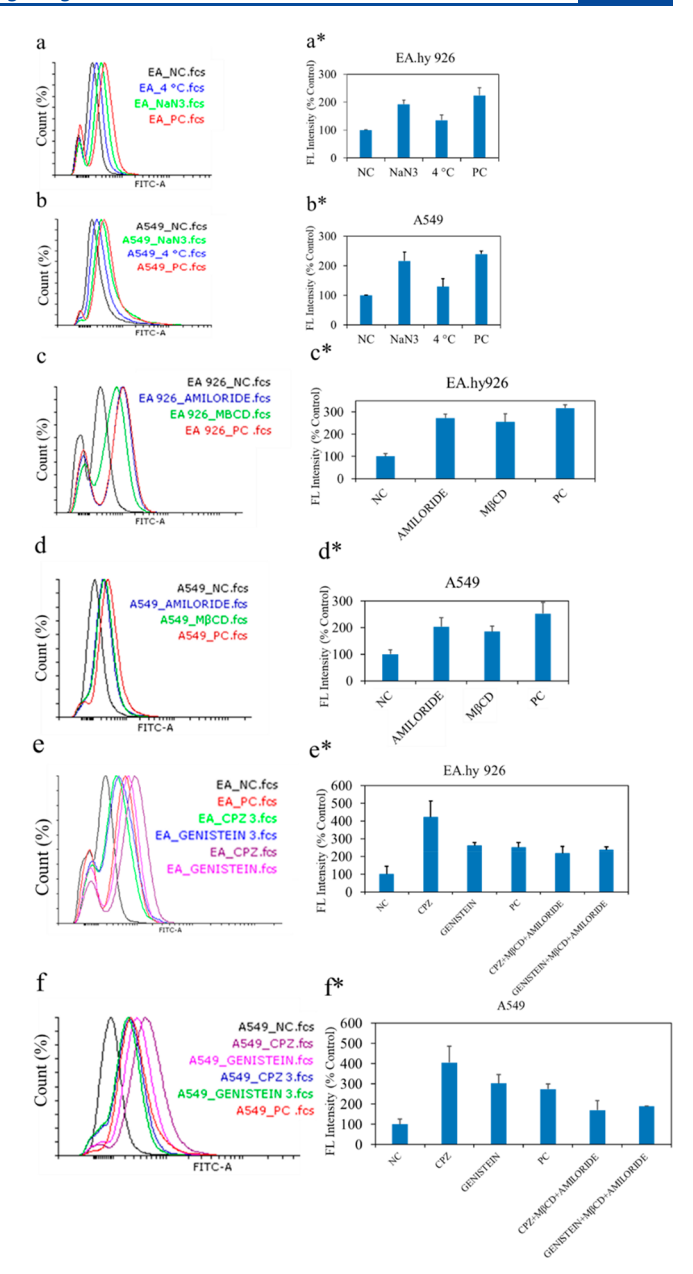
intensities of the blue channel and red channel, which could be simply represented by the gradient of the white line. Meanwhile, a more quantitative analysis of the subcellular location of the U-CNDs in the cells was done to get Pearson's correlation coefficient, 600 which is a measure of linear correlation between the location of U-CNDs and MitoTracker Red in cells. It turns out that the coefficient values for the CNDs-MitoTracker group in EA.hy926 and A549 cells were 0.79 and 0.43, respectively, suggesting the relatively more colocalization of the CNDs-MitoTracker in EA.hy926 cells than that in A549 cells.

To this end, it is necessary to further examine how the U-CNDs are taken up and transported within the cells. It is well accepted that the transport mechanisms in cells can be

grouped into three classes: simple diffusion, facilitated diffusion, and active transport. 61 Among them, simple diffusion and facilitated diffusion belong to energy-free movement, while active transport is energy-dependent movement. To determine the cellular uptake of the U-CNDs through either energydependent or -independent pathway, we examined the effects of temperature and ATP on this uptake process using flow cytometry method. Briefly, cells treated with CNDs were incubated at 4 °C or pretreated with NaN3 at 37 °C for 1 h. NaN<sub>3</sub> is known as a chemical which will block the endocytic pathways by disrupting ATP production. Figure 6a,b shows the intracellular fluorescence intensities of the cell treated with the U-CNDs at different conditions. The results show that the uptake amount of CNDs at 4 °C or presence of NaN<sub>3</sub> group decreased according to the less fluorescence intensities when compared to that of the positive control (PC), suggesting that the cellular uptake of the U-CNDs is somewhat temperature and ATP-dependent. One can conclude that the internalization of the U-CNDs is an endocytosis process associated with two facts: (1) the cellular uptake of the U-CNDs is energydependent, and (2) the CNDs are colocalized with mitochondria within the cells.

Next, we moved forward to test which specific endocytosis pathways are involved in the translocation of the U-CNDs. Four inhibitors, including chlorpromazine hydrochloride (CPZ: inhibitor of clathrin-mediated endocytosis (CME)), methyl- $\beta$ -cyclodextrins (M $\beta$ CD: inhibitor of lipid raft-mediated endocytosis (LrME)), amiloride (inhibitor of macropinocytosis), and genistein (inhibitor of caveolae-mediated endocytosis (CvME)), were chosen according to the inhibition functions. 46,62-64 After incubation for 24 h, cells were preincubated with one of the aforementioned endocytosis inhibitors dissolved in serum-free DMEM at 37 °C for 1 h and then incubated for another 3 h with the U-CNDs. Then the fluorescence intensity was analyzed using flow cytometer. It was observed that amiloride and M $\beta$ CD suppressed the internalization of CNDs, which is reflected by the decreased fluorescence intensity of U-CNDs in the cells (Figure 6c,d). The results imply that the internalization of U-CNDs is associated with macropinocytosis and lipid raft-mediated endocytosis. Notably, none of these pharmacological inhibitor treatments could fully block the uptake of CNDs, indicating that multiple pathways are involved in the U-CND internalization process simultaneously. CPZ and genistein surprisingly facilitated the internalization of CNDs instead of inhibiting the process, respectively, suggesting that the U-CNDs internalization unlikely involves in CME and CvME. And interestingly, the facilitation effect of CPZ and genistein was offset by the addition of amiloride and M $\beta$ CD (Figure 6e,f). Therefore, one could plausibly conclude that the macropinocytosis and lipid raft-mediated endocytosis of U-CNDs can be enhanced by the addition of CPZ and genistein. In summary, the internalization of the U-CNDs is temperature- and ATP-dependent and in favor of the macropinocytosis and lipid raft-mediated endocytosis pathways.

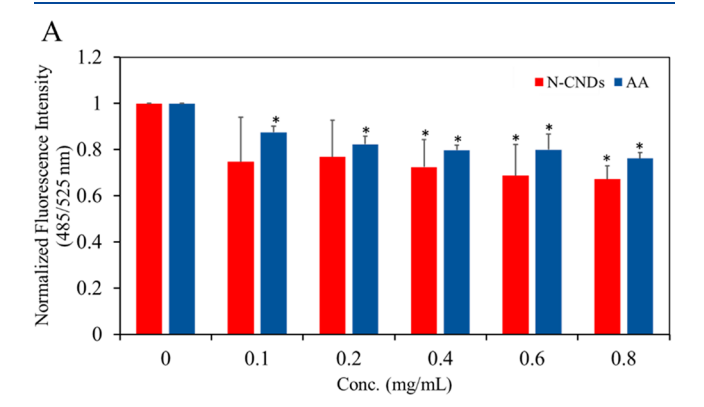
It is known that reactive oxygen species (ROS), including hydrogen peroxide  $(H_2O_2)$ , superoxide ion  $(O_2^-)$ , hydroxyl radical  $(OH^-)$ , *etc.*, is essential mediators in regulating various physiological functions of living organisms. <sup>65,66</sup> However, the overproduction of ROS causes the modification and damage of DNA, lipids, and cellular proteins, which will subsequently lead to cell death, and the onset of many degenerative diseases. <sup>67,68</sup> DCFH-DA was used to evaluate the intracellular ROS,



**Figure 6.** Flow cytometric graphs (parts a–f) and corresponding average fluorescence intensities (parts a\*-f\*) of CNDs in EA.hy926 and A549 cells. (a and b) Flow cytometric analyses of cells incubated at 4 °C or with NaN<sub>3</sub> at 37 °C. (c and d) Flow cytometric analyses of cells pretreated without (control) or with MβCD or amiloride before the introduction of CNDs. (e and f) Flow cytometric analyses of cells pretreated without (PC) or with CPZ, genistein, a mixture of CPZ with MβCD and amiloride, or mixture of genistein with MβCD and amiloride before the addition of CNDs. The concentration of CNDs at 0.8 mg/mL remained the same for all endocytosis experiments. PC: cells treated with CNDs without inhibitors. NC: cells without any treatment. CPZ 3: CPZ + MβCD + amiloride. GENISTEIN 3: genistein + MβCD + amiloride.

particularly  $H_2O_2$ , by a microplate reader in both cell lines. DCFH-DA is a cell-permeable and nonfluorescent probe, which could be hydrolyzed by esterases to the carboxylate anion (DCFH) intracellularly. Then the cellular oxidants could oxidize DCFH into fluorescent dichlorofluorescin (DCF), which could be traced either by a microplate reader or fluorescence microscope. The detected fluorescence intensity

represents the intracellular ROS (measured by H<sub>2</sub>O<sub>2</sub>) level. Figure 7 shows the decreased fluorescence intensity in both



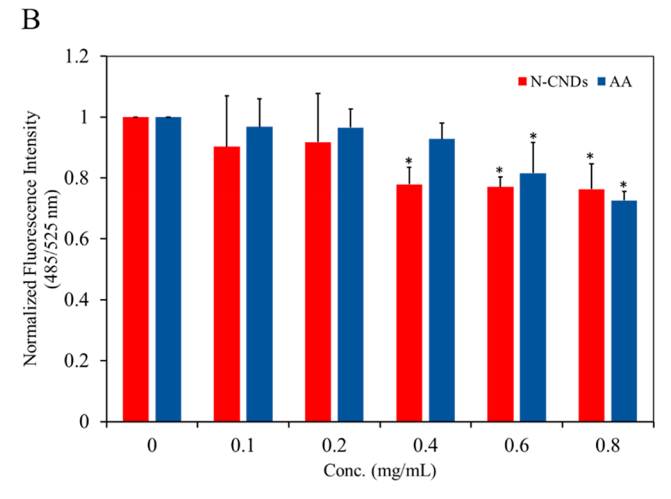


**Figure 7.** Effects of CNDs treatment on intracellular ROS production. ROS  $(H_2O_2)$  generation in EA.hy926 endothelial cells (A) and A549 cells (B) was monitored by DCFH-DA probe after 24 h of incubation with CNDs. Values are shown as mean  $\pm$  SD from three independent experiments. Triplicates of each treatment were performed in each independent experiment. \*p < 0.05 versus control (0 mg/mL).

cell lines upon the U-CND treatment, which proves the role of antioxidant of CNDs intracellularly. The data indicates the antioxidative effect of the U-CNDs is even better than ascorbic acid (AA), a well-known antioxidant.

# CONCLUSION

Herein, it is clearly demonstrated the U-CNDs render supreme biocompatibility in terms of cell morphology, viability, and metabolic activity upon uptake in both EA.hy926 cells and A549 cells. The high photoluminescence and strong antioxidative capacity in cells make the U-CNDs a good candidate in the applications of bioimaging and antioxidation fields. In addition, it was proved that the internalization of the U-CNDs is to some extent temperature- and ATP-dependent, mainly through macropinocytosis and lipid raft-mediated endocytosis pathways. Their subcellular localization in mitochondria implies their subsequent interaction within the cell's mitochondria and may attribute to the ROS scavenging capability. This work may promote further studies on the intracellular process and metabolic activities induced by the CNDs.

# ASSOCIATED CONTENT

# Supporting Information

The Supporting Information is available free of charge at https://pubs.acs.org/doi/10.1021/acs.langmuir.0c01598.

Additional U-CND characterization data and cell imaging (UV-vis, fluorescence, and confocal micrographs) (PDF)

# **■ AUTHOR INFORMATION**

# **Corresponding Author**

Jianjun Wei – Department of Nanoscience, Joint School of Nanoscience and Nanoengineering, University of North Carolina at Greensboro, Greensboro, North Carolina 27401, United States; ⊚ orcid.org/0000-0002-2658-0248; Phone: 1-336-285-2859; Email: j\_wei@uncg.edu

#### **Authors**

**Zuowei Ji** – Department of Nanoscience, Joint School of Nanoscience and Nanoengineering, University of North Carolina at Greensboro, Greensboro, North Carolina 27401, United States

Ziyu Yin — Department of Nanoscience, Joint School of Nanoscience and Nanoengineering, University of North Carolina at Greensboro, Greensboro, North Carolina 27401, United States

**Zhenquan Jia** — Department of Biology, University of North Carolina at Greensboro, Greensboro, North Carolina 27412, United States

Complete contact information is available at: https://pubs.acs.org/10.1021/acs.langmuir.0c01598

# **Author Contributions**

The manuscript was written with contributions by all authors. All authors have approved the final version of the manuscript.

### **Funding**

This work is supported by National Science Foundation (grant no. 1832134), National Institutes of Health (R15HL129212), and NC State fund through the Joint School of Nanoscience and Nanoengineering (JSNN).

# **Notes**

The authors declare no competing financial interest.

# ACKNOWLEDGMENTS

This work was performed at the JSNN, a member of Southeastern Nanotechnology Infrastructure Corridor (SENIC) and National Nanotechnology Coordinated Infrastructure (NNCI), which is supported by the National Science Foundation (ECCS-1542174).

# REFERENCES

- (1) Auffan, M.; Rose, J.; Bottero, J.-Y.; Lowry, G. V.; Jolivet, J.-P.; Wiesner, M. R. Towards a definition of inorganic nanoparticles from an environmental, health and safety perspective. *Nat. Nanotechnol.* **2009**, *4*, 634–641.
- (2) Millstone, J. E.; Kavulak, D. F. J.; Woo, C. H.; Holcombe, T. W.; Westling, E. J.; Briseno, A. L.; Toney, M. F.; Fréchet, J. M. J. Synthesis, Properties, and Electronic Applications of Size-Controlled Poly(3-hexylthiophene) Nanoparticles. *Langmuir* **2010**, *26*, 13056–13061.
- (3) Yu, H.; Li, L.; Zhang, Y. Silver nanoparticle-based thermal interface materials with ultra-low thermal resistance for power electronics applications. *Scr. Mater.* **2012**, *66*, 931–934.

- (4) Yeo, J.; Kim, G.; Hong, S.; Kim, M. S.; Kim, D.; Lee, J.; Lee, H. B.; Kwon, J.; Suh, Y. D.; Kang, H. W. Flexible supercapacitor fabrication by room temperature rapid laser processing of roll-to-roll printed metal nanoparticle ink for wearable electronics application. *J. Power Sources* **2014**, 246, 562–568.
- (5) Ning, F.; Shao, M.; Xu, S.; Fu, Y.; Zhang, R.; Wei, M.; Evans, D. G.; Duan, X. TiO2/graphene/NiFe-layered double hydroxide nanorod array photoanodes for efficient photoelectrochemical water splitting. *Energy Environ. Sci.* **2016**, *9*, 2633–2643.
- (6) Nie, H.; Li, M.; Li, Q.; Liang, S.; Tan, Y.; Sheng, L.; Shi, W.; Zhang, S. X.-A. Carbon dots with continuously tunable full-color emission and their application in ratiometric pH sensing. *Chem. Mater.* **2014**, *26*, 3104–3112.
- (7) Lin, X.; Gao, G.; Zheng, L.; Chi, Y.; Chen, G. Encapsulation of Strongly Fluorescent Carbon Quantum Dots in Metal—Organic Frameworks for Enhancing Chemical Sensing. *Anal. Chem.* **2014**, *86*, 1223—1228.
- (8) Nikalje, A. P. Nanotechnology and its applications in medicine. *Med. Chem.* **2015**, *5*, 081–089.
- (9) Hofmann-Amtenbrink, M.; Grainger, D. W.; Hofmann, H. Nanoparticles in medicine: Current challenges facing inorganic nanoparticle toxicity assessments and standardizations. *Nanomedicine* **2015**, *11*, 1689–1694.
- (10) Wang, R.; Zhang, F. NIR luminescent nanomaterials for biomedical imaging. *J. Mater. Chem. B* **2014**, *2*, 2422–2443.
- (11) Wang, Y.; Hu, A. Carbon quantum dots: synthesis, properties and applications. *I. Mater. Chem. C* **2014**, *2*, 6921–6939.
- (12) Li, H.; He, X.; Kang, Z.; Huang, H.; Liu, Y.; Liu, J.; Lian, S.; Tsang, C. H. A.; Yang, X.; Lee, S. T. Water-soluble fluorescent carbon quantum dots and photocatalyst design. *Angew. Chem., Int. Ed.* **2010**, 49, 4430–4434.
- (13) Zheng, X. T.; Ananthanarayanan, A.; Luo, K. Q.; Chen, P. Glowing Graphene Quantum Dots and Carbon Dots: Properties, Syntheses, and Biological Applications. *Small* **2015**, *11*, 1620–1636.
- (14) Kong, B.; Zhu, A.; Ding, C.; Zhao, X.; Li, B.; Tian, Y. Carbon Dot-Based Inorganic—Organic Nanosystem for Two-Photon Imaging and Biosensing of pH Variation in Living Cells and Tissues. *Adv. Mater.* **2012**, 24, 5844—5848.
- (15) Yang, Y.; Liu, J.; Guo, S.; Liu, Y.; Kang, Z. A nickel nanoparticle/carbon quantum dot hybrid as an efficient electrocatalyst for hydrogen evolution under alkaline conditions. *J. Mater. Chem. A* **2015**, *3*, 18598–18604.
- (16) Li, H.; He, X.; Kang, Z.; Huang, H.; Liu, Y.; Liu, J.; Lian, S.; Tsang, C. H. A.; Yang, X.; Lee, S.-T. Water-Soluble Fluorescent Carbon Quantum Dots and Photocatalyst Design. *Angew. Chem., Int. Ed.* **2010**, *49*, 4430–4434.
- (17) Wu, Z. L.; Zhang, P.; Gao, M. X.; Liu, C. F.; Wang, W.; Leng, F.; Huang, C. Z. One-pot hydrothermal synthesis of highly luminescent nitrogen-doped amphoteric carbon dots for bioimaging from Bombyx mori silk natural proteins. *J. Mater. Chem. B* **2013**, *1*, 2868—2873.
- (18) Liu, X.; Zhang, N.; Bing, T.; Shangguan, D. Carbon dots based dual-emission silica nanoparticles as a ratiometric nanosensor for Cu2+. *Anal. Chem.* **2014**, *86*, 2289–2296.
- (19) Shen, P.; Xia, Y. Synthesis-Modification Integration: One-Step Fabrication of Boronic Acid Functionalized Carbon Dots for Fluorescent Blood Sugar Sensing. *Anal. Chem.* **2014**, *86*, 5323–5329.
- (20) Kim, J.; Park, J.; Kim, H.; Singha, K.; Kim, W. J. Transfection and intracellular trafficking properties of carbon dot-gold nanoparticle molecular assembly conjugated with PEI-pDNA. *Biomaterials* **2013**, *34*, 7168–7180.
- (21) Huang, P.; Lin, J.; Wang, X.; Wang, Z.; Zhang, C.; He, M.; Wang, K.; Chen, F.; Li, Z.; Shen, G. Light-triggered theranostics based on photosensitizer-conjugated carbon dots for simultaneous enhanced-fluorescence imaging and photodynamic therapy. *Adv. Mater.* **2012**, *24*, 5104–5110.
- (22) Wang, Y.; Liang, Z.; Su, Z.; Zhang, K.; Ren, J.; Sun, R.; Wang, X. All-Biomass Fluorescent Hydrogels Based on Biomass Carbon

- Dots and Alginate/Nanocellulose for Biosensing. ACS Appl. Bio Mater. 2018, 1, 1398–1407.
- (23) Wang, Q.; Huang, X.; Long, Y.; Wang, X.; Zhang, H.; Zhu, R.; Liang, L.; Teng, P.; Zheng, H. Hollow luminescent carbon dots for drug delivery. *Carbon* **2013**, *59*, 192–199.
- (24) Choi, Y.; Kim, S.; Choi, M.-H.; Ryoo, S.-R.; Park, J.; Min, D.-H.; Kim, B.-S. Highly Biocompatible Carbon Nanodots for Simultaneous Bioimaging and Targeted Photodynamic Therapy In Vitro and In Vivo. *Adv. Funct. Mater.* **2014**, *24*, 5781–5789.
- (25) Gao, G.; Jiang, Y.-W.; Yang, J.; Wu, F.-G. Mitochondria-targetable carbon quantum dots for differentiating cancerous cells from normal cells. *Nanoscale* **2017**, *9*, 18368–18378.
- (26) Hua, X.-W.; Bao, Y.-W.; Chen, Z.; Wu, F.-G. Carbon quantum dots with intrinsic mitochondrial targeting ability for mitochondriabased theranostics. *Nanoscale* **2017**, *9*, 10948–10960.
- (27) Lee, H. U.; Park, S. Y.; Park, E. S.; Son, B.; Lee, S. C.; Lee, J. W.; Lee, Y.-C.; Kang, K. S.; Kim, M. I.; Park, H. G. Photoluminescent carbon nanotags from harmful cyanobacteria for drug delivery and imaging in cancer cells. *Sci. Rep.* **2015**, *4*, 4665.
- (28) Liu, C.; Zhang, P.; Zhai, X.; Tian, F.; Li, W.; Yang, J.; Liu, Y.; Wang, H.; Wang, W.; Liu, W. Nano-carrier for gene delivery and bioimaging based on carbon dots with PEI-passivation enhanced fluorescence. *Biomaterials* **2012**, *33*, 3604–3613.
- (29) Zhang, W.; Zeng, Z.; Wei, J. Electrochemical Study of DPPH Radical Scavenging for Evaluating the Antioxidant Capacity of Carbon Nanodots. *J. Phys. Chem. C* **2017**, *121*, 18635–18642.
- (30) Zhang, W.; Chavez, J.; Zeng, Z.; Bloom, B.; Sheardy, A.; Ji, Z.; Yin, Z.; Waldeck, D. H.; Jia, Z.; Wei, J. Antioxidant Capacity of Nitrogen and Sulfur Codoped Carbon Nanodots. *ACS Appl. Nano Mater.* **2018**, *1*, 2699–2708.
- (31) Xu, J.; Li, F.; Wang, D.; Nawaz, M. H.; An, Q.; Han, D.; Niu, L. Co3O4 nanostructures on flexible carbon cloth for crystal plane effect of nonenzymatic electrocatalysis for glucose. *Biosens. Bioelectron.* **2019**, 123, 25–29.
- (32) Ji, Z.; Arvapalli, D. M.; Zhang, W.; Yin, Z.; Wei, J. Nitrogen and sulfur co-doped carbon nanodots in living EA.hy926 and A549 cells: oxidative stress effect and mitochondria targeting. *J. Mater. Sci.* **2020**, 55, 6093–6104.
- (33) Zeng, Q.; Shao, D.; He, X.; Ren, Z.; Ji, W.; Shan, C.; Qu, S.; Li, J.; Chen, L.; Li, Q. Carbon dots as a trackable drug delivery carrier for localized cancer therapy in vivo. *J. Mater. Chem. B* **2016**, *4*, 5119–5126.
- (34) Sharma, A.; Das, J. Small molecules derived carbon dots: synthesis and applications in sensing, catalysis, imaging, and biomedicine. *J. Nanobiotechnol.* **2019**, *17*, 92.
- (35) Zeng, Z.; Zhang, W.; Arvapalli, D. M.; Bloom, B.; Sheardy, A.; Mabe, T.; Liu, Y.; Ji, Z.; Chevva, H.; Waldeck, D. H.; Wei, J. A fluorescence-electrochemical study of carbon nanodots (CNDs) in bio- and photoelectronic applications and energy gap investigation. *Phys. Chem. Chem. Phys.* **2017**, *19*, 20101–20109.
- (36) Zhu, S.; Zhao, X.; Song, Y.; Lu, S.; Yang, B. Beyond bottom-up carbon nanodots: Citric-acid derived organic molecules. *Nano Today* **2016**, *11*, 128–132.
- (37) Sharma, A.; Gadly, T.; Gupta, A.; Ballal, A.; Ghosh, S. K.; Kumbhakar, M. Origin of Excitation Dependent Fluorescence in Carbon Nanodots. *J. Phys. Chem. Lett.* **2016**, *7*, 3695–3702.
- (38) Schneider, J.; Reckmeier, C. J.; Xiong, Y.; von Seckendorff, M.; Susha, A. S.; Kasák, P.; Rogach, A. L. Molecular Fluorescence in Citric Acid-Based Carbon Dots. *J. Phys. Chem. C* **2017**, *121*, 2014–2022.
- (39) Strauss, V.; Margraf, J. T.; Dolle, C.; Butz, B.; Nacken, T. J.; Walter, J.; Bauer, W.; Peukert, W.; Spiecker, E.; Clark, T.; Guldi, D. M. Carbon Nanodots: Toward a Comprehensive Understanding of Their Photoluminescence. *J. Am. Chem. Soc.* **2014**, *136*, 17308–17316.
- (40) Kasprzyk, W.; Świergosz, T.; Bednarz, S.; Walas, K.; Bashmakova, N. V.; Bogdał, D. Luminescence phenomena of carbon dots derived from citric acid and urea—a molecular insight. *Nanoscale* **2018**, *10*, 13889–13894.

- (41) Simões, E. F.; Leitão, J. M.; da Silva, J. C. E. Carbon dots prepared from citric acid and urea as fluorescent probes for hypochlorite and peroxynitrite. *Microchim. Acta* **2016**, *183*, 1769–1777.
- (42) Devi, J. S. A.; Aparna, R. S.; Aswathy, B.; Nebu, J.; Aswathy, A. O.; George, S. Understanding the Citric Acid—Urea Co—Directed Microwave Assisted Synthesis and Ferric Ion Modulation of Fluorescent Nitrogen Doped Carbon Dots: A Turn On Assay for Ascorbic Acid. *Chemistry Select* **2019**, *4*, 816—824.
- (43) Wang, T.; Wang, A.; Wang, R.; Liu, Z.; Sun, Y.; Shan, G.; Chen, Y.; Liu, Y. Carbon dots with molecular fluorescence and their application as a "turn-off" fluorescent probe for ferricyanide detection. *Sci. Rep.* **2019**, *9*, 10723.
- (44) Qu, S.; Wang, X.; Lu, Q.; Liu, X.; Wang, L. A Biocompatible Fluorescent Ink Based on Water-Soluble Luminescent Carbon Nanodots. *Angew. Chem., Int. Ed.* **2012**, *51*, 12215–12218.
- (45) Koivusalo, M.; Welch, C.; Hayashi, H.; Scott, C. C.; Kim, M.; Alexander, T.; Touret, N.; Hahn, K. M.; Grinstein, S. Amiloride inhibits macropinocytosis by lowering submembranous pH and preventing Rac1 and Cdc42 signaling. *J. Cell Biol.* **2010**, *188*, 547–563.
- (46) Vercauteren, D.; Vandenbroucke, R. E.; Jones, A. T.; Rejman, J.; Demeester, J.; De Smedt, S. C.; Sanders, N. N.; Braeckmans, K. The Use of Inhibitors to Study Endocytic Pathways of Gene Carriers: Optimization and Pitfalls. *Mol. Ther.* **2010**, *18*, 561–569.
- (47) Hao, X.; Wu, J.; Shan, Y.; Cai, M.; Shang, X.; Jiang, J.; Wang, H. Caveolae-mediated endocytosis of biocompatible gold nanoparticles in living Hela cells. *J. Phys.: Condens. Matter* **2012**, *24*, 164207.
- (48) dos Santos, T.; Varela, J.; Lynch, I.; Salvati, A.; Dawson, K. A. Effects of Transport Inhibitors on the Cellular Uptake of Carboxylated Polystyrene Nanoparticles in Different Cell Lines. *PLoS One* **2011**, *6*, No. e24438.
- (49) Cuong, T. V.; Pham, V. H.; Tran, Q. T.; Hahn, S. H.; Chung, J. S.; Shin, E. W.; Kim, E. J. Photoluminescence and Raman studies of graphene thin films prepared by reduction of graphene oxide. *Mater. Lett.* **2010**, *64*, 399–401.
- (50) Luo, Z.; Lu, Y.; Somers, L. A.; Johnson, A. T. C. High Yield Preparation of Macroscopic Graphene Oxide Membranes. *J. Am. Chem. Soc.* **2009**, *131*, 898–899.
- (51) Arvapalli, D. M.; Sheardy, A. T.; Alapati, K. C.; Wei, J. High Quantum Yield Fluorescent Carbon Nanodots for detection of Fe (III) Ions and Electrochemical Study of Quenching Mechanism. *Talanta* **2020**, 209, 120538.
- (52) Schroeder, Elizabeth A.; Raimundo, N.; Shadel, Gerald S. Epigenetic Silencing Mediates Mitochondria Stress-Induced Longevity. *Cell Metab.* **2013**, *17*, 954–964.
- (53) Ahn, C. S.; Metallo, C. M. Mitochondria as biosynthetic factories for cancer proliferation. *Cancer Metab.* **2015**, *3*, 1.
- (54) Marchi, S.; Patergnani, S.; Missiroli, S.; Morciano, G.; Rimessi, A.; Wieckowski, M. R.; Giorgi, C.; Pinton, P. Mitochondrial and endoplasmic reticulum calcium homeostasis and cell death. *Cell Calcium* **2018**, *69*, *62*–72.
- (55) Wu, D.; Ma, Y.; Cao, Y.; Zhang, T. Mitochondrial toxicity of nanomaterials. Sci. Total Environ. 2020, 702, 134994.
- (56) Zulian, A.; Schiavone, M.; Giorgio, V.; Bernardi, P. Forty years later: Mitochondria as therapeutic targets in muscle diseases. *Pharmacol. Res.* **2016**, *113*, 563–573.
- (57) Wang, X.; Wang, W.; Li, L.; Perry, G.; Lee, H.-g.; Zhu, X. Oxidative stress and mitochondrial dysfunction in Alzheimer's disease. *Biochim. Biophys. Acta, Mol. Basis Dis.* **2014**, *1842*, 1240–1247.
- (58) Dorn, G. W. Mitochondrial dynamics in heart disease. *Biochim. Biophys. Acta, Mol. Cell Res.* **2013**, 1833, 233–241.
- (59) Kim, J.; Moody, J. P.; Edgerly, C. K.; Bordiuk, O. L.; Cormier, K.; Smith, K.; Beal, M. F.; Ferrante, R. J. Mitochondrial loss, dysfunction and altered dynamics in Huntington's disease. *Hum. Mol. Genet.* **2010**, *19*, 3919–3935.
- (60) Pearson's Correlation Coefficient. In *Encyclopedia of Public Health*; Kirch, W., Ed. Springer Netherlands: Dordrecht, 2008; pp 1090–1091.

- (61) Mosquera, J. s.; García, I.; Liz-Marzán, L. M. Cellular uptake of nanoparticles versus small molecules: A matter of size. *Acc. Chem. Res.* **2018**, *51*, 2305–2313.
- (62) Wang, H.-Y.; Hua, X.-W.; Jia, H.-R.; Liu, P.; Gu, N.; Chen, Z.; Wu, F.-G. Enhanced cell membrane enrichment and subsequent cellular internalization of quantum dots via cell surface engineering: illuminating plasma membranes with quantum dots. *J. Mater. Chem. B* **2016**, *4*, 834–843.
- (63) Bareford, L. M.; Swaan, P. W. Endocytic mechanisms for targeted drug delivery. Adv. Drug Delivery Rev. 2007, 59, 748-758.
- (64) Wei, T.; Chen, C.; Liu, J.; Liu, C.; Posocco, P.; Liu, X.; Cheng, Q.; Huo, S.; Liang, Z.; Fermeglia, M.; Pricl, S.; Liang, X.-J.; Rocchi, P.; Peng, L. Anticancer drug nanomicelles formed by self-assembling amphiphilic dendrimer to combat cancer drug resistance. *Proc. Natl. Acad. Sci. U. S. A.* 2015, 112, 2978–2983.
- (65) Circu, M. L.; Aw, T. Y. Reactive oxygen species, cellular redox systems, and apoptosis. *Free Radical Biol. Med.* **2010**, 48, 749–762.
- (66) Schieber, M.; Chandel, Navdeep S. ROS Function in Redox Signaling and Oxidative Stress. *Curr. Biol.* **2014**, *24*, R453–R462.
- (67) Manoharan, S.; Guillemin, G. J.; Abiramasundari, R. S.; Essa, M. M.; Akbar, M.; Akbar, M. D. The Role of Reactive Oxygen Species in the Pathogenesis of Alzheimer's Disease, Parkinson's Disease, and Huntington's Disease: A Mini Review. *Oxid. Med. Cell. Longevity* **2016**, 2016, 8590578–8590578.
- (68) Verbon, E. H.; Post, J. A.; Boonstra, J. The influence of reactive oxygen species on cell cycle progression in mammalian cells. *Gene* **2012**, *511*, 1–6.